ELSEVIER

International Journal of Heat and Fluid Flow 19 (1998) 401–417

International Journal of HEAT AND FLUID FLOW

Combined heat and mass transfer in a uniformly heated vertical tube with water film cooling

S. He, P. An, J. Li, J.D. Jackson *

School of Engineering, University of Manchester, Simon Building, Oxford Road, Manchester M13 9PL, UK

Abstract

A computational study is reported of buoyancy-influenced forced upward turbulent flow of air and water vapour in the range of Reynolds number from 4600 to 13 800 within a long uniformly heated vertical tube in the presence of a falling film of water on the inside wall. Procedures have been successfully developed which enable this complex problem to be simulated using turbulence modelling and an elliptical computational scheme. Simulations have been made for a range of conditions and detailed comparisons are made with experiments. Useful progress has been made in understanding the fluid dynamics and thermal physics involved. Within the first 20 diameters, the effects of the re-organisation of the flow and turbulence field dominate. Within this region, turbulence entering with the imposed flow decays away, a new turbulence structure is generated in the wall region and this propagates into the core further downstream. The sensible Nusselt number in this region is generally lower than it is in the upper section of the tube. Both the mean and the turbulent fields are affected by buoyancy under certain conditions. In extreme cases, the flow is laminarised and heat transfer considerably impaired. Two very different modes of heat transfer were identified. When the cooling water is supplied at relatively high temperature, the system operates in the *evaporation mode*. Energy supplied by the wall is mainly absorbed by evaporation of water from the film. The water temperature and the conditions of the flow are important factors controlling the effectiveness of heat transfer under such conditions. In contrast, when the temperature at which the water is supplied is relatively low the system operates in the *direct film cooling mode*. Convection of heat by the flowing water film becomes the main mechanism for heat removal from the tube.

Keywords: Heat and mass transfer; Falling water film cooling; Buoyancy influence; Mixed convection; Turbulence modelling

Notation

Bo	buoyancy parameter defined by Eq. (18)
c_p	specific heat
d	diameter of the tube
D	mass diffusivity
g	acceleration due to gravity
Gr	Grashof number based on $\beta g d^4 q_{tot}/k\nu^2$
Gr′	Grashof number based on $((\rho_b - \rho_w)/\rho_b)(gd^3/\nu^2)$
k	turbulence kinetic energy
$\dot{m}$	mass flow rate
M	molecular weight
Nu_s	sensible Nusselt number, Eq. (19)
p	pressure
Pr	Prandtl number, $\mu C_p/\lambda$
q_{mc}	heat flux due to convection of air/vapour mixture
q_{ev}	heat flux due to evaporation from the water film
q_{tot}	heat flux from the tube
q_{wc}	heat flux due to convection in water film
r	radial co-ordinate
R	radius of the tube
Re	Reynolds number based on mass flow rate
Re_e	effective Reynolds number defined by Eq. (16)
Re_f	water film Reynolds number
Re_t	turbulence Reynolds number, $k^2/\nu\tilde{\epsilon}$
Sc	Schmidt number, ν/D
T	temperature
U	longitudinal velocity
U_b	bulk velocity
V	radial velocity
x	longitudinal co-ordinate
y	radial co-ordinate measured from the wall

Greek

δ	water film thickness
ϵ	dissipation of turbulence energy
γ	latent heat
λ	thermal conductivity
μ	dynamic viscosity
ν	kinematic viscosity
ρ	density
σ	turbulent Prandtl number
ω	vapour concentration

Subscripts

b	bulk

* Corresponding author.

0142-727X/98/$ – see front matter
PII: S0142-727X(98)10021-8

0 inlet
e evaporation
I interface
v vapour
m air/vapour mixture

1. Introduction

Passive cooling, involving flow which is induced naturally due to density variation, is an inherently reliable way to remove heat from a system. It has a number of important applications in both engineering and natural systems. One which is currently of particular interest is the cooling by naturally induced air flow over the outside of the steel container vessel of an advanced light water nuclear reactor. However, in some situations, this mechanism alone might not be sufficient to remove heat effectively from a system and to keep the temperature of it below the required level. One measure which could be adopted to enhance the effectiveness of cooling under such situations is to allow a water film to flow downwards over the hot surface of the system, so as to exploit the high effectiveness of heat transfer by evaporation.

Computational studies of water film cooling have been carried out by a number of investigators. Examples include the work on combined heat and mass transfer in laminar natural convection from a vertical wall by Gebhart and Pera (1971) and flow along a vertical cylinder by Chen and Yuh (1980). Both utilised the Boussinesq approximation, which enabled the governing equations to be reduced to a form which had a similarity solution. The flow was treated in a similar manner to one involving a single mechanism of buoyancy influence. In an interesting study of natural convection flow in an open vertical tube, resulting from the combined buoyancy effects arising from both thermal and mass diffusion, Chang et al. (1986) solved the Navier–Stokes equations using the thin shear flow assumptions. The wall of the tube was considered to be covered by a stationary water film at a specified uniform temperature. This study was extended later by Chiang and Kleinstreuer (1991) by allowing the liquid film to fall under the action of gravity and removing the thin shear flow assumptions. Both studies involved the Boussinesq approximation and the flow was assumed to be laminar. Studies of combined heat and mass transfer in natural convection between two vertical parallel plates with film evaporation were made by Yan and Lin (1990), again for laminar flow. Recently, Fedorov et al. (1997) published a study of the same problem but with a turbulent flow. The water film was considered as being stationary and, in most of the calculations, buoyancy influences were neglected. Yan and Soong (1995) considered an inclined plate with film cooling and evaporation. The flow was considered to be turbulent in both the water and gas phases and was solved for both regions. A modified Van Driest mixing length was used for the water film and a k–ϵ turbulence model for the vapour and gas flow region. The calculations were for conditions of forced convection and the thin shear flow assumption was employed.

Combined experimental and computational studies of buoyancy-influenced turbulent flow of air and water vapour within a long uniformly heated vertical tube in the presence of a falling film of water on the inside wall have recently been completed by the present authors (see Jackson et al., 1998) in connection with the evaluation of ideas for the passive cooling of advanced, inherently safe, nuclear reactors. The computational study, which utilised an elliptic finite volume/finite difference scheme incorporating a low Reynolds number turbulence model, is reported in this paper and comparisons are made with the authors' experimental data. The fluid flow and heat transfer physics involved in the problem are discussed in some detail in the light of the results of the simulations.

2. Modelling

2.1. General remarks

The arrangement used in the associated experimental study involved a long vertical stainless steel tube (76 mm inside diameter and 8 m long), which was heated in a uniform manner along the whole of its length by passing electrical current through it. Radial jets of water were sprayed onto the inside surface of the tube near the top, so as to form a thin film which ran down the wall. A forced upward flow of air and vapour was created in the tube by supplying air from a compressor to a settling box at the bottom of the tube, where it had a bell-mouth intake. The top of the tube was open to the atmosphere. A sketch of the test section is shown in Fig. 1. In the experimental programme, the water and gas flow rates, the temperature of the inlet water and the electrical power input to the heated section of the tube were systematically varied. The measurements of the tube wall temperature distribution were made using thermocouples attached to the outside.

In order to simulate the experiments, the governing equations for the turbulent flow, heat and mass transfer in the air/vapour mixture were solved using a finite volume method using an elliptic scheme. Incorporated in these equations was the Launder–Sharma low Reynolds number k–ϵ turbulence model (Launder and Sharma, 1974). The motion of the downward flowing water film was determined analytically assuming that the shear on it exerted by the flow of the air/vapour mixture could be neglected. The temperature field within the water film was computed by solving the energy equation for that region simultaneously with that for the air/vapour field.

The simplifying assumptions concerning the water film flow were based on the following arguments. The water film flows downward primarily under the action of gravity. In theory it can be influenced by the flow of the air/vapour mixture but the effects can be shown to be negligibly small under the

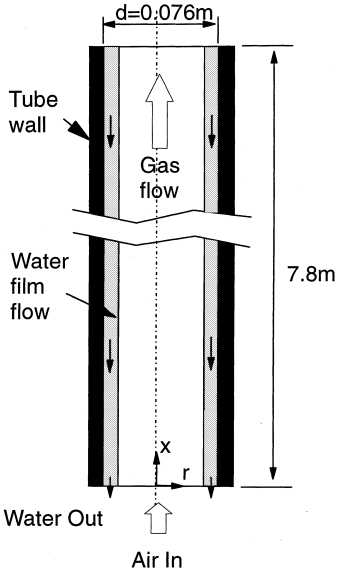

Fig. 1. Test section.

present experimental conditions. Thus, the water film flow can be decoupled from that of the air/vapour mixture. The Reynolds number of the water film flow ($\mathrm{Re_f} = 4\dot{m}_f/\pi D\mu$) was no more than 452, which is much lower than the critical value of 1500 for laminar conditions quoted by Ueda and Tanaka (1975). The water film flow was therefore assumed to be laminar. Under such conditions, the following analytical solution for the velocity distribution in the water is applicable

$$U = \frac{\rho g}{\mu}\left(\delta y - \frac{y^2}{2}\right) \tag{1}$$

in which δ is the water film thickness ($= [3\dot{m}v/\pi d\rho g]^{1/3}$).

2.2. Governing equations

The flow is considered to be incompressible and axisymmetric. The Reynolds averaged equations for such a flow written in cylindrical co-ordinates are:

Continuity

$$\frac{1}{r}\left\{\frac{\partial}{\partial x}(\rho r U) + \frac{\partial}{\partial r}(\rho r V)\right\} = 0, \tag{2}$$

U-momentum

$$\frac{1}{r}\left\{\frac{\partial}{\partial x}(\rho r U^2) + \frac{\partial}{\partial r}(\rho r V U)\right\} = -\frac{\partial p}{\partial x} + \rho g + \frac{1}{r}\left\{2\frac{\partial}{\partial x}\left[r\mu_e\left(\frac{\partial U}{\partial x}\right)\right] + \frac{\partial}{\partial r}\left[r\mu_e\left(\frac{\partial U}{\partial r} + \frac{\partial V}{\partial x}\right)\right]\right\}, \tag{3}$$

V-momentum

$$\frac{1}{r}\left\{\frac{\partial}{\partial x}(\rho r U V) + \frac{\partial}{\partial r}(\rho r V^2)\right\} = -\frac{\partial p}{\partial r} + \frac{1}{r}\left\{\frac{\partial}{\partial x}\left[r\mu_e\left(\frac{\partial V}{\partial x} + \frac{\partial U}{\partial r}\right)\right] + 2\frac{\partial}{\partial r}\left[r\mu_e\left(\frac{\partial V}{\partial r}\right)\right]\right\} - 2\frac{\mu_e V}{r^2} \tag{4}$$

in which μ_e is the effective viscosity defined by $\mu_e = \mu + \mu_T$, where μ_T is the turbulent viscosity, and ρ the density.

The energy equation for axisymmetric flow written using cylindrical co-ordinates is shown below. It can be used for both the water and gas flows:

Energy equation

$$\frac{1}{r}\left\{\frac{\partial}{\partial x}(\rho r U T) + \frac{\partial}{\partial r}(\rho r V T)\right\} = \frac{1}{r}\left\{\frac{\partial}{\partial x}\left[r\left(\frac{\mu}{\mathrm{Pr}} + \frac{\mu_T}{\sigma_T}\right)\frac{\partial T}{\partial x}\right] + \frac{\partial}{\partial r}\left[r\left(\frac{\mu}{\mathrm{Pr}} + \frac{\mu_T}{\sigma_T}\right)\frac{\partial T}{\partial r}\right]\right\}, \tag{5}$$

Pr is the molecular Prandtl number and σ_T the turbulent Prandtl number. For the water phase flow, $\mu_T = 0$ (laminar flow). The vapour mass transport equation for axisymmetric flow written in cylindrical co-ordinates, is as follows:

Mass transfer equation

$$\frac{1}{r}\left\{\frac{\partial}{\partial x}(\rho r U \omega) + \frac{\partial}{\partial r}(\rho r V \omega)\right\} = \frac{1}{r}\left\{\frac{\partial}{\partial x}\left[r\left(\frac{\mu}{\mathrm{Sc}} + \frac{\mu_T}{\sigma_\omega}\right)\frac{\partial \omega}{\partial x}\right] + \frac{\partial}{\partial r}\left[r\left(\frac{\mu}{\mathrm{Sc}} + \frac{\mu_T}{\sigma_\omega}\right)\frac{\partial \omega}{\partial r}\right]\right\}, \tag{6}$$

Sc is the Schmidt number and σ_ω the turbulent Schmidt number. The vapour fraction ω is defined as the ratio of the density of the vapour to the overall density of the air/vapour mixture.

2.3. Turbulence model

At low values of air vapour mixture flow rate in the present study, convection was strongly modified due to buoyancy and non-uniformity of fluid properties. Simple turbulence models involving the use of wall functions were not applicable. A low-Reynolds number turbulence model incorporating parameters dependent on the local conditions is needed to describe such flows. The low Reynolds number k–ϵ turbulence model due to Launder and Sharma (1974) has been found in earlier work carried out by the present authors to perform well in some mixed convection flows (see for example, Jackson et al., 1993) and has therefore been used here. The details of the model are presented below:

Constitutive Equation

$$\mu_T = C_\mu f_\mu \rho k^2/\tilde{\varepsilon}, \tag{7}$$

k-transport

$$\frac{1}{r}\left\{\frac{\partial}{\partial x}(\rho r U k) + \frac{\partial}{\partial r}(\rho r V k)\right\} = \frac{1}{r}\left\{\frac{\partial}{\partial x}\left[r\left(\mu + \frac{\mu_T}{\sigma_k}\right)\frac{\partial k}{\partial x}\right] + \frac{\partial}{\partial r}\left[r\left(\mu + \frac{\mu_T}{\sigma_k}\right)\frac{\partial k}{\partial r}\right]\right\} + P_k - \rho\varepsilon, \tag{8}$$

ϵ-transport

$$\frac{1}{r}\left\{\frac{\partial}{\partial x}(\rho r U \tilde{\varepsilon}) + \frac{\partial}{\partial r}(\rho r V \tilde{\varepsilon})\right\} = \frac{1}{r}\left\{\frac{\partial}{\partial x}\left[r\left(\mu + \frac{\mu_T}{\sigma_\varepsilon}\right)\frac{\partial \tilde{\varepsilon}}{\partial x}\right] + \frac{\partial}{\partial r}\left[r\left(\mu + \frac{\mu_T}{\sigma_\varepsilon}\right)\frac{\partial \tilde{\varepsilon}}{\partial r}\right]\right\} + C_{\varepsilon 1}\frac{\tilde{\varepsilon}}{k}P_k - C_{\varepsilon 2} f_2 \rho\frac{\tilde{\varepsilon}^2}{k} + E, \tag{9}$$

where:

$$\tilde{\varepsilon} = \varepsilon - D, \quad P_k = \mu_T G,$$

$$G = 2\left(\frac{\partial U}{\partial x}\right)^2 + 2\left(\frac{\partial V}{\partial r}\right)^2 + 2\left(\frac{V}{r}\right)^2 + \left(\frac{\partial U}{\partial r} + \frac{\partial V}{\partial x}\right)^2,$$

Constants and functions

$$C_\mu = 0.09, \quad C_{\epsilon 1} = 1.44, \quad C_{\epsilon 2} = 1.92,$$

$$\sigma_k = 1.0, \quad \sigma_\epsilon = 1.3, \quad \sigma_T = 0.9,$$

$$f_\mu = \exp\left[-3.5/(1 + \mathrm{Re_t}/50)^2\right],$$

$$f_2 = 1 - 0.3\,\exp(-\mathrm{Re_t^2}), \qquad D = 2\nu\left[\left(\frac{\partial k^{1/2}}{\partial x}\right)^2 + \left(\frac{\partial k^{1/2}}{\partial r}\right)^2\right],$$

$$E = 2\frac{\mu\mu_t}{\rho}\left[\left(\frac{\partial^2 U}{\partial x^2}\right)^2 + \left(\frac{\partial^2 U}{\partial r^2}\right)^2 + 2\left(\frac{\partial^2 U}{\partial x\,\partial r}\right)^2 + \left(\frac{\partial^2 V}{\partial x^2}\right)^2 + \left(\frac{\partial^2 V}{\partial r^2}\right)^2 + 2\left(\frac{\partial^2 V}{\partial x\,\partial r}\right)^2\right],$$

$$\mathrm{Re_t} = k^2/\nu\tilde{\varepsilon}.$$

2.4. Boundary conditions

2.4.1. Air/vapour mixture flow

In view of the fact that a well designed bell-mouth intake was used in the experimental arrangement, it was considered appropriate to assume that the inlet flow conditions could be described using uniform profiles. However, some calculations using different assumptions concerning the inlet conditions, such as that of fully developed turbulent pipe flow or flow with reduced turbulence level, have also been carried out to test the sensitivity of the results to the assumed condition. The effects of varying such parameters on wall temperature were generally found to be small and confined to the first few diameters of the flow. At the exit from the pipe, where the air–vapour mixture leaves the system, the zero gradient condition was used for all variables. A summary of the boundary conditions is given below:

$$
\begin{aligned}
&x = 0: \quad U = U_0, \quad V = 0, \quad T = T_0,\\
&\omega = \omega_{\mathrm{sab}} \quad k = (0.01U_0)^2, \quad \tilde{\varepsilon} = C_\mu k_0^{3/2}/0.03R,\\
&x = L: \quad \frac{\partial U}{\partial x} = 0, \quad V = 0, \quad \frac{\partial T}{\partial x} = 0,\\
&\frac{\partial \omega}{\partial x} = 0, \quad \frac{\partial k}{\partial x} = 0, \quad \frac{\partial \tilde{\varepsilon}}{\partial x} = 0,\\
&r = 0: \quad \frac{\partial U}{\partial r} = 0, \quad V = 0, \quad \frac{\partial T}{\partial r} = 0,\\
&\frac{\partial \omega}{\partial r} = 0, \quad \frac{\partial k}{\partial r} = 0, \quad \frac{\partial \tilde{\varepsilon}}{\partial r} = 0.
\end{aligned}
\tag{10}
$$

2.4.2. Water film flow

For the water film flow, the only boundary conditions required are those for temperature and they are:

$$
\begin{aligned}
&x = L: \quad T = T_{\mathrm{water,in,}}\\
&x = 0: \quad \frac{\partial T}{\partial x} = 0,\\
&r = R: \quad k\frac{\partial T}{\partial r} = q_0.
\end{aligned}
\tag{11}
$$

2.4.3. Boundary conditions at the interface

(a) The vapour fraction at the interface: On the assumption of thermodynamic equilibrium, the vapour pressure takes its saturated value corresponding to the local temperature at the interface. The vapour mass fraction there can therefore be calculated using

$$\omega_i = \frac{M_{\mathrm{v}} p_{\mathrm{v}}}{M_{\mathrm{v}} p_{\mathrm{v}} + M_{\mathrm{a}}(p - p_{\mathrm{v}})}, \tag{12}$$

where p and p_{v} are the total pressure and the vapour pressure at the interface, respectively. M_{a} and M_{v} are the molecular weights of air and vapour.

(b) Velocity of the air/vapour mixture at the interface: The axial component of velocity is calculated using Eq. (1). The radial velocity component is non-zero due to the generation of vapour at the interface. Assuming that the gas–water interface is semi-permeable (that is, the solubility of air into the water is negligibly small so that the air does not move radially at the interface), the velocity of water vapour at the interface can be written as

$$v_i = -\frac{D}{(1-\omega_i)}\frac{\partial \omega}{\partial y}\bigg|_{\mathrm{interface}} \tag{13}$$

in which D is the mass diffusivity.

(c) Energy balance at the interface: At the interface, energy conservation requires that the difference between the heat diffused on each side is equal to the energy used in the evaporation of vapour at the interface. Thus

$$\lambda_{\mathrm{water}}\frac{\partial T}{\partial y}\bigg|_{\delta^-} - \lambda_{\mathrm{gas}}\frac{\partial T}{\partial y}\bigg|_{\delta^+} = \dot{m}\gamma \tag{14}$$

in which γ is the enthalpy of evaporation and $\dot{m}$, the vapour generation rate ($= \rho_{\mathrm{vapour}} v_i$).

(d) Turbulence parameters at the interface: Since the water flow is assumed to be steady and laminar, we treat the water–gas interface as a solid wall with transpiration; that is, we set the conditions

$$k = 0, \quad \tilde{\varepsilon} = 0. \tag{15}$$

2.5. Numerical method

The transport differential equations for both the mean flow parameters and turbulent parameters were discretized using the widely used finite volume scheme (Patankar, 1981). The complete computational domain was discretized into a mesh of grids, typically, 72×62. Mesh dependence was checked by doubling the grid size. In the radial direction, the mesh was uniform in the water phase but was compressed towards the wall in the air/vapour mixture phase. In the axial direction, it was compressed towards the flow gas inlet. The strategy adopted for generation of control volumes was the grid point centred one, i.e., the control volume faces were first defined and the grid point was placed in the centre of the control volume. The staggered grid arrangement was used for the storage of the variables. The scalar parameters were stored at the grid points and the velocity components were stored in the control volume surfaces. The QUICK scheme was used for approximating the convection terms in the momentum equations. This approach ensured relatively good accuracy. The UP-WIND scheme was used for other transport equations for reasons of numerical stability. The SIMPLE scheme was used for coupling the pressure and the velocity fields. The resulting algebraic coefficient matrix system was solved iteratively using the line-by-line TDMA algorithm. For all the variables except temperature, the computations were carried out only in the gas phase. The velocity distribution in the water phase was calculated using Eq. (1). Since the temperature fields in the water film and the air mixture were closely coupled, the calculation for temperature was carried out simultaneously for both regions.

It is worth noting that particular care was needed in the computational treatment of the boundary conditions at the interface. The arrangement adopted in this study for the interfacial cells and the neighbouring cells is shown in Fig. 2. For variables other than temperature, cell NJ − 1 is the cell at which boundary conditions are taken into account. For the case of energy equation, cells NJ − 1, NJ and NJ + 1 are internal; yet they need special treatment. Cells NJ − 1 and NJ + 1 are similar to ordinary boundary cells in the sense that they have one of their neighbouring grid points locating at the corresponding cell face, otherwise they are treated like other internal cells. The cell NJ is defined so that it is infinitesimal in the radial direction. Under such conditions, the convection term is negligible. The discretised energy equation for the cell NJ is simply a finite difference form of the interfacial condition, Eq. (14).

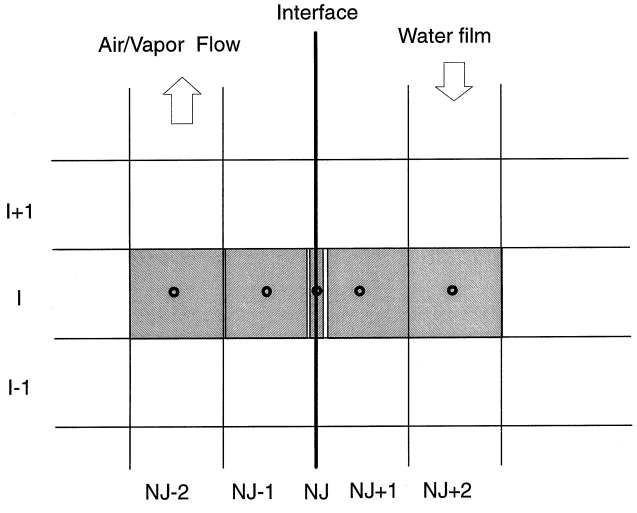

Fig. 2. Arrangement of cells at the water/gas flow interface.

Table 1
Conditions of the simulations

Run	Power (W)	Air flow			Water flow			Inlet buoyancy parameter
		Reynolds number (Re)	Flow rate (kg/s)	Inlet fluid temp. (°C)	Reynolds number (Re_f)	Flow rate (kg/s)	Inlet fluid temp. (°C)	
2	1350	13 800	0.015	30	452	0.027	70	0.84
3	3000	13 800	0.015	30	452	0.027	70	1.23
4	3000	13 800	0.015	30	218	0.013	66	1.34
5	1350	13 800	0.015	30	218	0.013	66	1.36
7	1350	13 800	0.015	20	452	0.027	17	0.24
8	5000	13 800	0.015	30	452	0.027	80	1.60
9	1350	13 800	0.015	30	452	0.027	40	0.55
10	1350	13 800	0.015	30	452	0.027	53	0.74
11	1350	9200	0.010	30	452	0.027	71	2.63
12	1350	4600	0.005	30	452	0.027	73	12.0
14	3000	4600	0.005	30	452	0.027	76	15.8
16	1350	4600	0.005	30	452	0.027	40	6.7

3. Results

A summary of the conditions of the experiments (Jackson et al., 1998) which have been simulated in the study is shown in Table 1. The water and gas flow rates, the temperature of the inlet water and the power input to the flow from the heated tube were systematically varied to investigate their effects. In some cases, the inlet conditions have been varied in the simulations in order to test the sensitivity of the results to those parameters.

It is worth clarifying some of the terms used in the discussion before presenting the results

Effective Reynolds number: In the present study, the velocity is negative at the interface between the falling liquid film and the air/vapour phase. The conventional Reynolds number based on mass flow rate ($4\dot{m}/\pi\mu d = \rho U_b d/\mu$) needs to be modified in order to take account of this. We define an effective Reynolds number based on a modified characteristic velocity, $U_b - U_i = U_b + |U_i|$, i.e.,

$$Re_e = \rho_b(U_b - U_i)d/\mu_b \tag{16}$$

in which ρ_b and μ_b are mass weighted density and dynamic viscosity of the air/vapour mixture, respectively.

Buoyancy parameter: The parameter proposed by Jackson and Hall (1979) to quantify the buoyancy effect for single phase mixed convection in a heated tube is defined as

$$Bo = \frac{8 \times 10^4\ Gr}{Re^{3.425}}\ Pr^{0.8}, \tag{17}$$

where $Gr = \beta g d^4 q/kv^2$. In this study we utilise this concept. But for the case of water film cooling, we need to use a slightly modified form, which is based on the density difference to account for buoyancy effects in the mixture caused by both the non-uniformity of the temperature and the vapour concentration, i.e.,

$$Bo = \frac{8 \times 10^4\ Gr'}{Re_e^{2.625}\ Pr^{0.8}}, \tag{18}$$

where $Gr' = ((\rho_b - \rho_i)/\rho_b)(gd^3/v^2)$ in which ρ_i is the mixture density at the interface and ρ_b, the mixture mass weighted mean density.

Sensible Nusselt number: In the case of water film cooling, two mechanisms are involved in the energy transfer between the interface and the air/vapour mixture phase, i.e., energy transfer by means of convection (sensible heat transfer) and energy used for evaporation of liquid from the water film (latent heat transfer). In particular, Nusselt number based on sensible heat flux will be used in the discussion of the results and described as sensible Nusselt number

$$Nu_s = \frac{q_{mc} d}{k_m}. \tag{19}$$

Flow laminarisation: The term 'partial laminarisation' is used here to indicate a situation where there is a significant reduction of the turbulence intensity in comparison with its normal level, say, more than 20%, due to reasons, such as, buoyancy influence or flow acceleration. We describe the flow being 'laminarised' if the turbulence intensity is reduced to an extremely low level.

3.1. Comparisons between measured wall temperature distributions and simulations

Fig. 3 shows comparisons between predicted distributions of wall temperature along the tube and those measured in the experiments for a number of conditions. Referring first to Fig. 3(a), the air flow rate was varied, whilst other conditions, such as, the power input and mass flow rate and temperature of the cooling water, were kept fixed. Run 14 is an exception. In that case the power input was doubled and the Reynolds number was kept low to investigate the effects of buoyancy. Fig. 3(b) shows the effects of varying the power input and the mass flow rate of water supplied and Fig. 3(c) shows the effect of varying the inlet temperature of the cooling water. It is clear that generally the simulations do reproduce observed behaviour quite well. However, in Fig. 3(a) an exception is apparent in the case of the lowest air flow rate (run 12). The computed wall temperature is clearly too high. It appears that in the simulation for this case, the turbulence model overresponded to buoyancy influences causing the flow to be almost completely laminarised (see Section 3.2). This resulted in the predicted effectiveness of the heat transfer being significantly lower than that which actually prevailed. The results of a simulation for this condition with buoyancy effects switched off are also shown in the figure as run 12a. In this simulation the flow remained turbulent and the calculated distribution of temperature was close to the measured one. Now we turn our attention to run 14 the experimental conditions of which are the same as those of run 12 apart from the power input being more than doubled. For this case, the buoyancy effect is significant and the flow is actually laminarised. Under these conditions, as can be seen from the figure, the predicted wall temperature agrees well with the measurement.

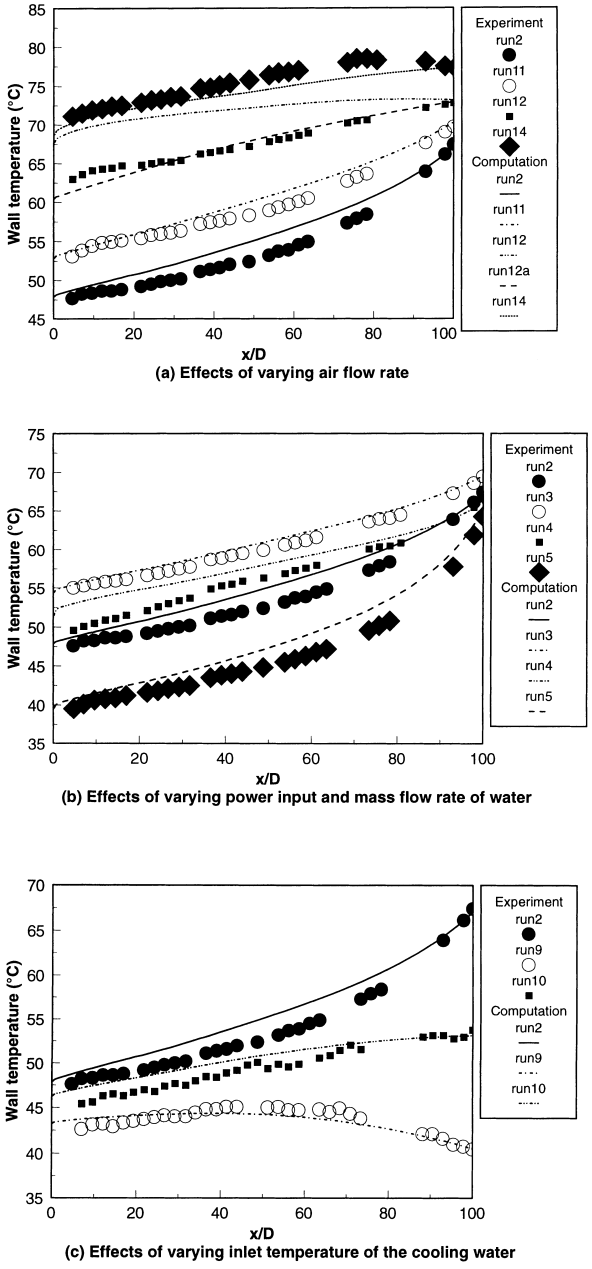

Fig. 3. Variation of wall temperature along the tube – comparisons of predictions with experiments.

3.2. Fluid dynamics

3.2.1. Reynolds number and buoyancy parameter

Fig. 4 shows the variation of the effective Reynolds number of the air/vapour mixture flow along the tube for various cases. It can be seen that the Reynolds number may either increase or decrease along the tube depending on the experimental conditions. It is apparent that the trend is mainly dependent on the level of wall temperature. When the wall temperature is high, the Reynolds number increases along the tube. This behaviour can be contrasted with the trend in the case of single phase flowof air in a heated tube. For such a flow, the Reynolds number will always decrease as the fluid temperature increases. This is due to the increase of the dynamic viscosity as can be seen from the formulation of the Reynolds number, $\mathrm{Re} = 4\dot{m}/\pi D\mu$. For such flows, the higher the wall temperature, the greater is the increase of the temperature of the fluid and, therefore, the greater is the reduction of the Reynolds number. For the case of flow with evaporation of water from a film, although the dynamic viscosity still increases with temperature, the mass flow rate also increases due to the build up of vapour, which is taking place. When the wall temperature level is high, the net effect is to cause the Reynolds number to increase with axial position. When the temperature of the wall is low, such as in runs 7 and 16, the evaporation is not so strong and the net effect is that the Reynolds number decreases in the flow direction.

Fig. 5 shows the variation of the buoyancy parameter along the tube in the flow direction. A semi-logarithmic scale is used in order to cover all the cases on a single diagram. Comparing Figs. 3 and 5, it can be seen that the effect of increase of the wall temperature is to increase the buoyancy parameter. However, for a fixed Reynolds number, this effect is limited by the fact that the maximum temperature of the fluid cannot exceed the saturation temperature. For example, for runs with flows of $\mathrm{Re} = 13\,800$, the buoyancy parameter is always low. The effect on buoyancy parameter of reducing Reynolds number is more pronounced. When the Reynolds number is reduced from 138 000 to 4600, the buoyancy parameter is increased by approximately 18 times. As a matter of fact, apart from the cases with the lowest effective Reynolds number, the influence of the buoyancy is always small and the heat transfer regime is that of forced convection.

It is of interest to note that the buoyancy parameter falls with distance along the tube in most cases as the bulk temperature of the fluid increases (Fig. 6). This again is in contrast with what occurs in single phase flow of air in a heated tube. For that case the buoyancy parameter always increases with bulk temperature, which can be seen from its definition.

It can also be seen from Fig. 5 that the buoyancy parameter becomes negative in the upper part of the tube in runs 7, 9 and 16. The condition changes from being buoyancy-assisted to buoyancy-opposed as we progress up the tube. Therefore in the upper section of the tube, the wall temperature is actually below the bulk fluid temperature.

3.2.2. Mean velocity field

Fig. 7 shows the development of the predicted normalised velocity profiles along the tube for various cases. Although the bulk velocity may vary considerably according to the experimental conditions, the normalised velocity profiles are rather similar for most of the cases (except for run 14). The most noticeable feature is the initial development of the velocity profile near the entrance. The imposed uniform inlet velocity profile gradually adapts itself to a developed turbulent one. This always takes about 20 diameters irrespective of Reynolds number.

The effect of buoyancy on velocity distribution is strong when the temperature difference between the wall and the fluid is large and the Reynolds number is low. Under such conditions, the velocity profile are modified considerably, as can be seen in the case shown in Fig. 7(e) (run 14). The velocity profile tends to take on a shape, typical of what is found in single phase mixed convection with strong buoyancy influences with peaks occurring at some radial location and a minimum at the centre (Jackson and Li, 1995).

3.2.3. Turbulence intensity

Fig. 8 shows the development of the computed radial distribution of turbulence intensity in the axial direction for a number of cases with higher Reynolds number. Fig. 9 shows the development of turbulence intensity in the flow direction for various radial positions. It can be seen that the trend is very similar in all the cases shown. The turbulence in the near wall

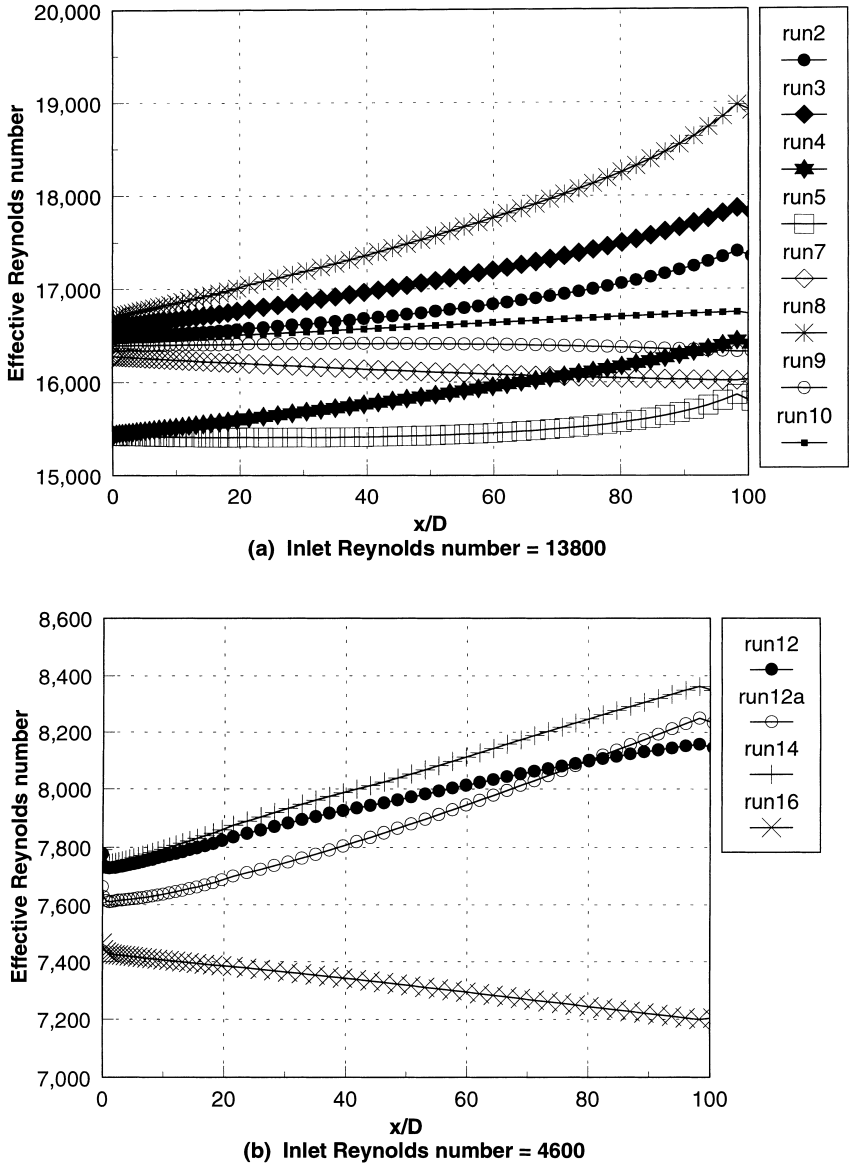

Fig. 4. Variations of the effective Reynolds number of mixture along the tube.

region responds to the new conditions. This response propagates towards the core of the tube as we proceed downstream. Turbulence intensity in the buffer region ($5 < y^+ < 30$), see for example Fig. 9(a) for the case of $y/R = 0.04$ ($y^+ = 20$ at inlet), starts to increase as soon as the flow enters the tube and the major changes are completed within less than five diameters. For a position in the core region, the development of turbulence intensity is much slower and occurs in two stages. In the first stage, the turbulence energy decays exponentially. In the second stage, turbulence intensity increases rapidly and reaches its final level within a relatively short distance. The further away the location is from the wall, the longer is the first stage.

As shown in Fig. 5, the buoyancy parameter for this group of experiments is relatively low and as expected, the effect of buoyancy on turbulence is not strong. Still, some effect can be seen in the core of the tube in downstream region of the flow, for instance in Fig. 9. Turbulence seems to be impaired in runs 2, 3 and 8, the buoyancy parameters of which are the largest. Turbulence intensity is highest in runs 7 and 9. In these cases, the effect of buoyancy on turbulence is reversed in the upper part of the tube and turbulence production is enhanced, but generally only by a small amount.

Fig. 10 shows the development of the radial profiles of turbulent intensity along the tube for test cases with Reynolds number of 4600. Fig. 11 shows the axial development of turbulent intensity at four chosen radial positions for the same test cases. As the Reynolds number is small, the buoyancy effect is more pronounced.

The buoyancy effect is the strongest in run 14. In this case, the flow is predicted to be partially laminarised. Turbulence energy decays in the near wall region, where, in turbulent shear flow, it is normally generated. Some turbulence is generated in the core region as a result of the occurrence of negative velocity gradient in that region caused by the influence of buoyancy (see Fig. 7(e)). Turbulence then decreases in the later stages as the buoyancy influence decreases.

The behaviour in run 16 is of particular interest. The flow starts by being buoyancy-assisted with a rather strong buoyancy influence but it develops to a buoyancy-opposed flow in

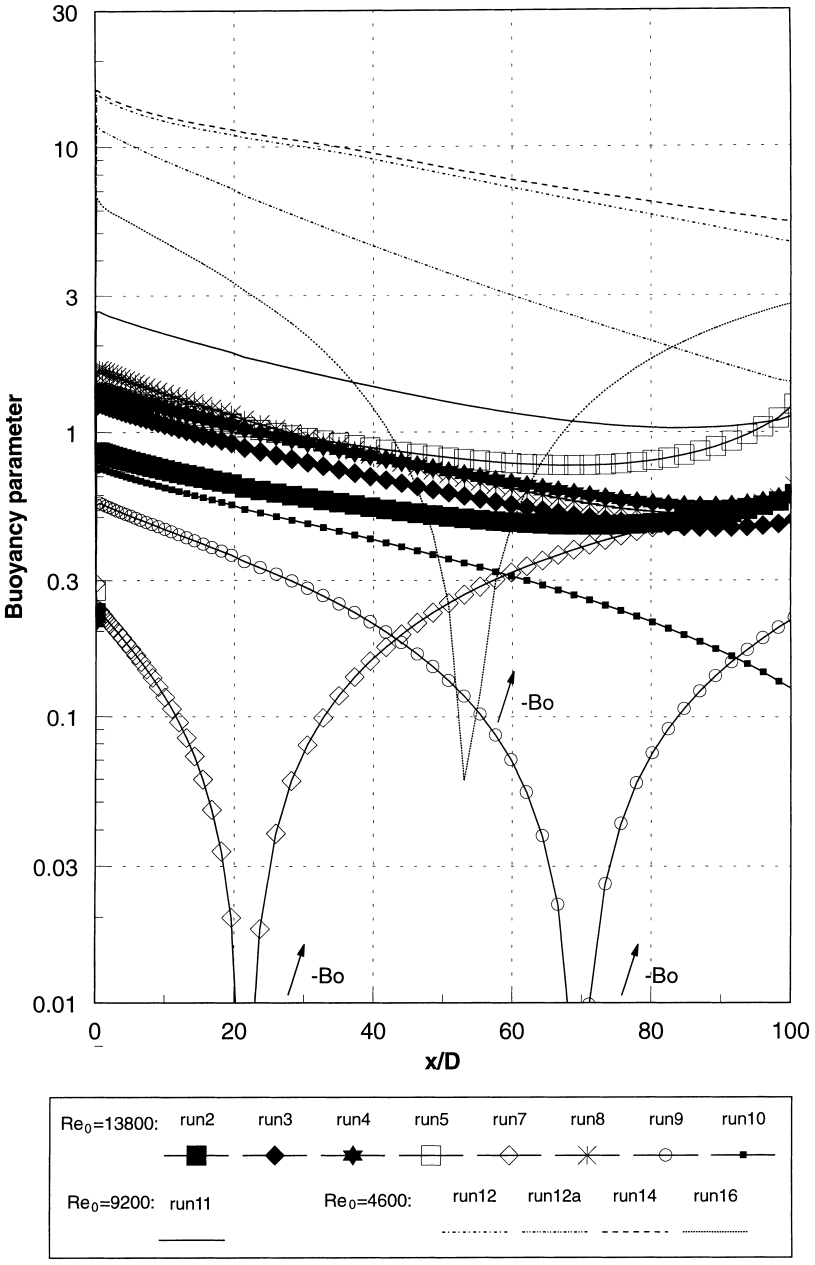

Fig. 5. Variations of the buoyancy parameter along the tube.

the upper section of the tube. The temperature difference between the wall and the bulk fluid reverses there. The difference between the response of turbulence in the upper part of the tube in this case and that in the cases shown in Fig. 9 is clear. While the turbulence approaches constant in the upper part of the tube in the other cases, it increases continuously in the case of run 16.

The predicted development of turbulence intensity in the case of run 12 is almost identical to that of run 14. The flow is predicted to be partially laminarised. However, as shown in Fig. 3, the predicted wall temperature is much higher than that measured. It seems that whereas the flow is not significantly laminarised in practice, it is in the simulation. In fact, the measured wall temperature variation is rather similar to the one predicted with the buoyancy effect completely suppressed (setting the buoyancy term to zero) in the simulation run 12a. Under such conditions, the development of turbulence intensity is rather similar to that in other cases with lower buoyancy effect. Under such conditions, the Launder Sharma-low-Reynolds number turbulence model has over-responded to the buoyancy influence and predicted the onset of laminarisation too early.

3.3. Thermal physics

3.3.1. Heat transfer modes

In the case of heat transfer with water film cooling, three major mechanisms are involved, (a) energy transport into the air/vapour mixture by means of convection (sensible heat transfer), (b) energy used to evaporate water from the liquid film (latent heat transfer) and (c) convection of heat in the water film due to its change of temperature as it flows along

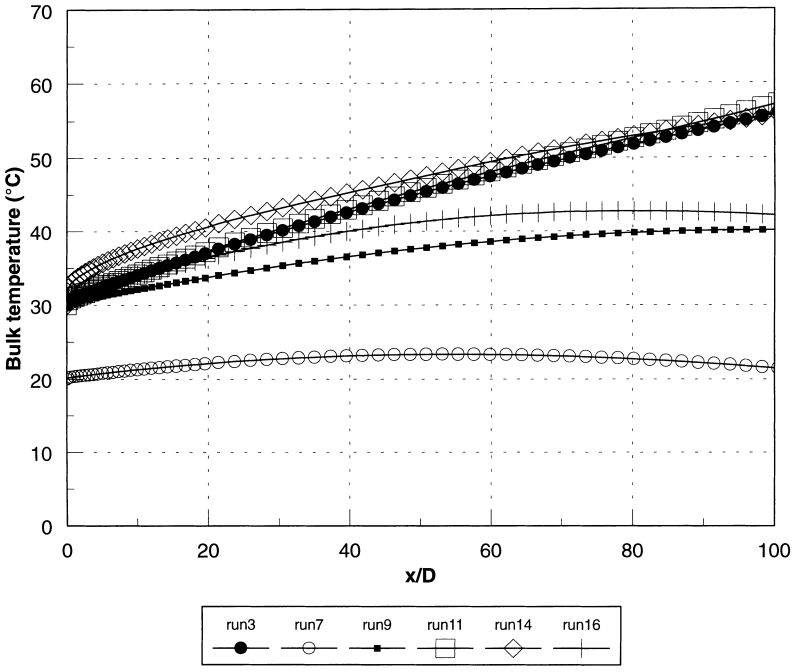

Fig. 6. Variations of the bulk temperature along the tube.

the wall (direct water film cooling). The contribution of each of those mechanisms can be positive (if its effect is to reduce the temperature of the wall) or negative (if otherwise). One of the useful pieces of information provided by a computational simulation is an energy budget. We consider an element of the system of unit length with one surface coinciding with the wall and the other with the air–water interface, the energy balance can be expressed as

Heat released from wall to water film (q_{tot})
+ Convection of heat in flowing water film (q_{wc})
+ Energy used in evaporation (q_{ev})
+ Energy transfer by the air/vapour mixture due to convection (q_{mc}) = 0.

Heat fluxes due to each of those mechanisms can be calculated as follows using results from the simulations:

$$q_{tot} = -k_{water}\left.\frac{\partial T}{\partial y}\right|_{wall},$$
$$q_{mc} = k_{air}\left.\frac{\partial T}{\partial y}\right|_{interface/gas\text{-}flow\text{-}side},$$
$$q_{wc} = \int_{interface}^{wall} 2\pi r\rho C_p U\frac{\partial T}{\partial x}\,dr, \qquad (20)$$
$$q_{ev} = -\left(\rho_{vapour}\gamma V\right)_{interface/gas\text{-}flow\text{-}side}.$$

Fig. 12 shows such energy transfers for chosen cases. Two very different patterns of behaviour can be seen from the figure. When the temperature of the water at the inlet is high (such as runs 3, 11 and 14), the saturated vapour pressure at the water-gas mixture interface is high, which means that there is plenty of evaporation of water, and therefore very effective heat transfer from the wall through that mechanism. Evaporation of the water film thus serves as the main mechanism for heat removal from the water. The temperature of the water decreases as it runs down the wall and the contribution of convection in the water to heat removal from the wall is negative, i.e., the water actually releases energy to the core flow as it flows down the wall. We will describe the system as working in the *evaporation mode*. In contrast, when the water at inlet is at relatively low temperature such as in run 7, the saturated vapour pressure is low and evaporation ceases to be a major mechanism for heat removal from the wall. The heat released by the wall is mainly carried away by the falling water film itself. Only a small portion of the heat released by the wall is transferred into the air/vapour mixture. In an extreme situation, that heat transfer even reverses. We describe such a system as working in the *direct film cooling mode*. Under such conditions an increase of mass flow rate of water will cause a reduction of wall temperature. There are also situations where both evaporation heat transfer and convection in the water flow are important (runs 9 and 16).

3.3.2. Convective and evaporative heat transfer

For both the modes discussed above, the heat removal which can be directly attributed to heat transfer into the air/vapour mixture by diffusion of heat at the interface is small. However, the turbulent diffusion process in the air/vapour mixture is of importance when the system is working in the *evaporation mode*. Under such conditions, the rate of evaporation of liquid from the interface depends on the rate at which the vapour is transferred away from it. The transport process itself is then dependent on the flow conditions. The effectiveness of such mass transfer can be represented by the Sherwood number. The latter can be directly related to sensible Nusselt number using heat and mass transfer analogy. The latter can therefore be used to indicate the effectiveness of the heat transfer due to both the convection and evaporation.

Fig. 13 shows the variation of the sensible Nusselt number along the tube for various test cases. The effect of the Reynolds number on sensible Nusselt number is known. The higher the Reynolds number, the higher is the Nusselt number. For cases with higher Reynolds number the buoyancy parameter Bo is relatively small and the effect of the buoyancy is not significant. The variation of sensible Nusselt number is very similar

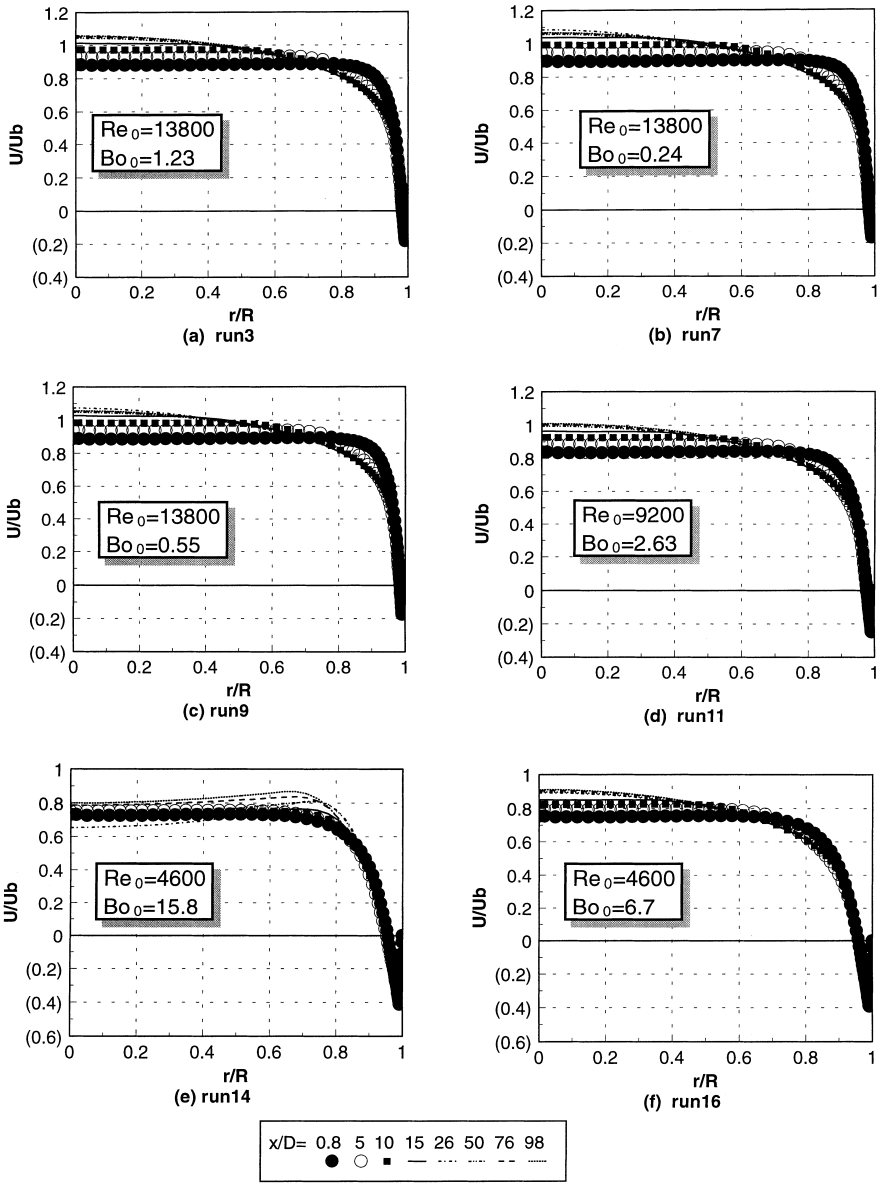

Fig. 7. Development of the velocity profiles.

in all such cases. It drops fast from a very high value to a level below its final value, after which there is a small but abrupt local rise followed by a gradual increase to its final value at about $x/d = 40$. Two major factors are responsible for this variation. The development of the thermal boundary layer which starts from zero thickness is responsible for the initial fast fall of the Nusselt number. The response of turbulence in the wall region is mainly responsible for the variation of the Nusselt number in the later stage. As shown in Fig. 9(a), turbulence intensity increases abruptly within the first few diameters. It then continues to increase gradually until about $x/d = 40$. This is clearly consistent with the variation of the Nusselt number. It can be seen that significant deviations from the trend described above occur in runs 7 and 9. In these cases, the wall temperature approaches the bulk temperature of the air/vapour mixture at some location, and consequently, the Nusselt number becomes large.

In the case of low Reynolds number, the effect of buoyancy is very pronounced. In the extreme situation, the flow can be laminarised, as in run 14. This is clearly reflected in the values of the Nusselt number. For that case, it is reduced to about one-third of that for forced convection under corresponding conditions of flow rate. Both the convective heat transfer from the interface and that due to evaporation are considerably impaired.

It is worth noticing that the increase of the wall temperature caused by the laminarisation of the flow is less in the case of water film cooling than it would be in a single phase convection situation. In the latter case, under conditions of flow laminarisation, the wall temperature increase can be large and result in over-heating. However, in the case of water film cooling, the increase of the wall temperature is limited. There are two reasons, both of which are relevant to the increase of the temperature of the water which accompanies the increase of the temperature of the wall. Firstly, when the temperature of water increases, it absorbs energy and the convection by the water flow increases accordingly. This in turn helps to keep the temperature of the wall down. The larger the mass flow

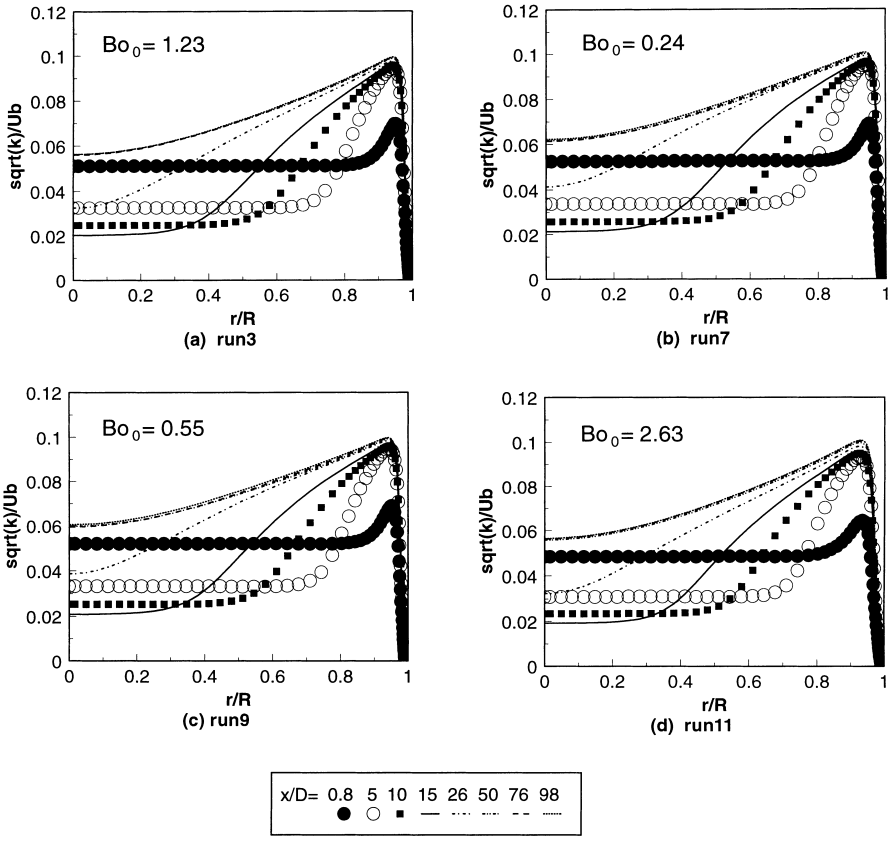

Fig. 8. Development of radial distribution of turbulence intensity – higher Reynolds number cases ($Re_0 = 13\,800$).

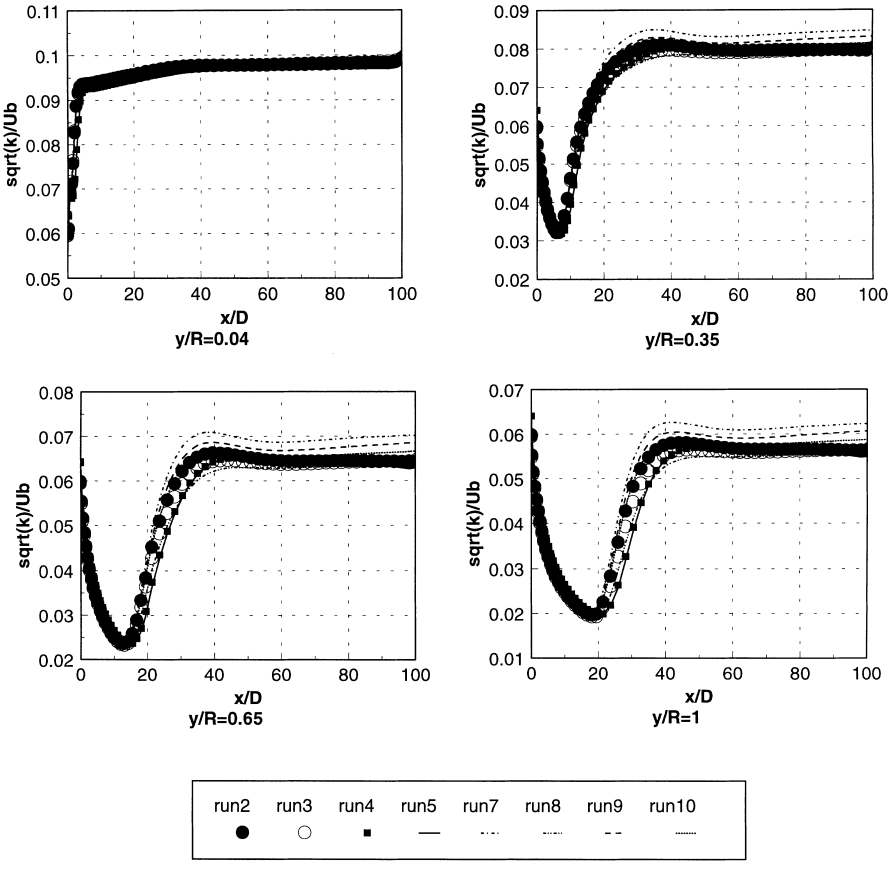

Fig. 9. Variations along the tube of turbulence intensity at chosen radial positions – higher Reynolds number cases ($Re_0 = 13\,800$).

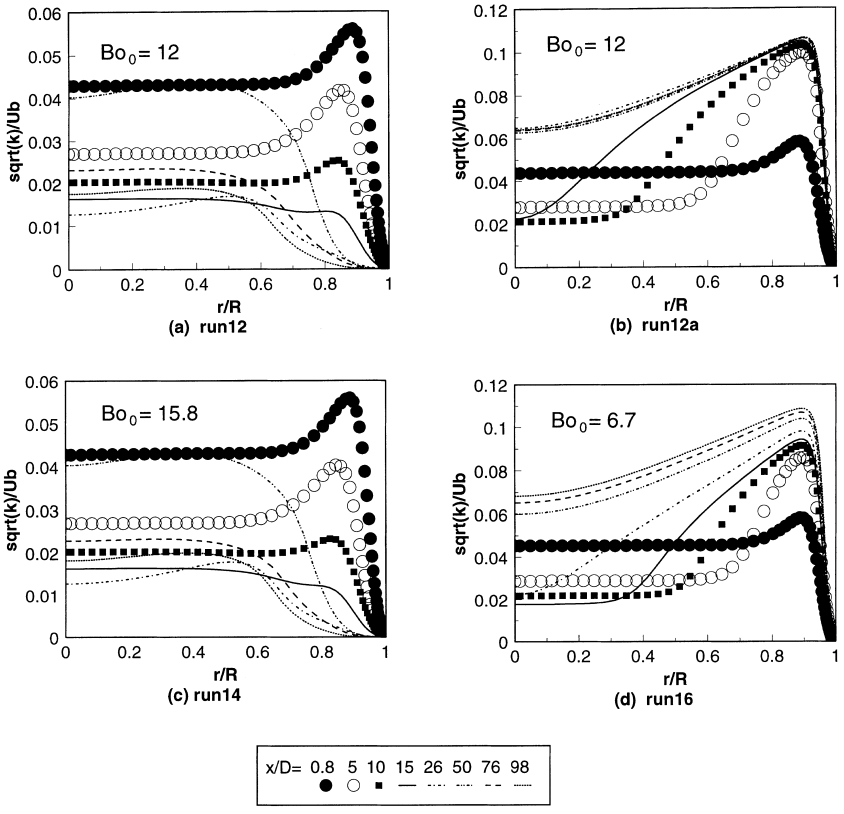

Fig. 10. Development of radial distribution of turbulence intensity – lower Reynolds number cases ($Re_0 = 4600$).

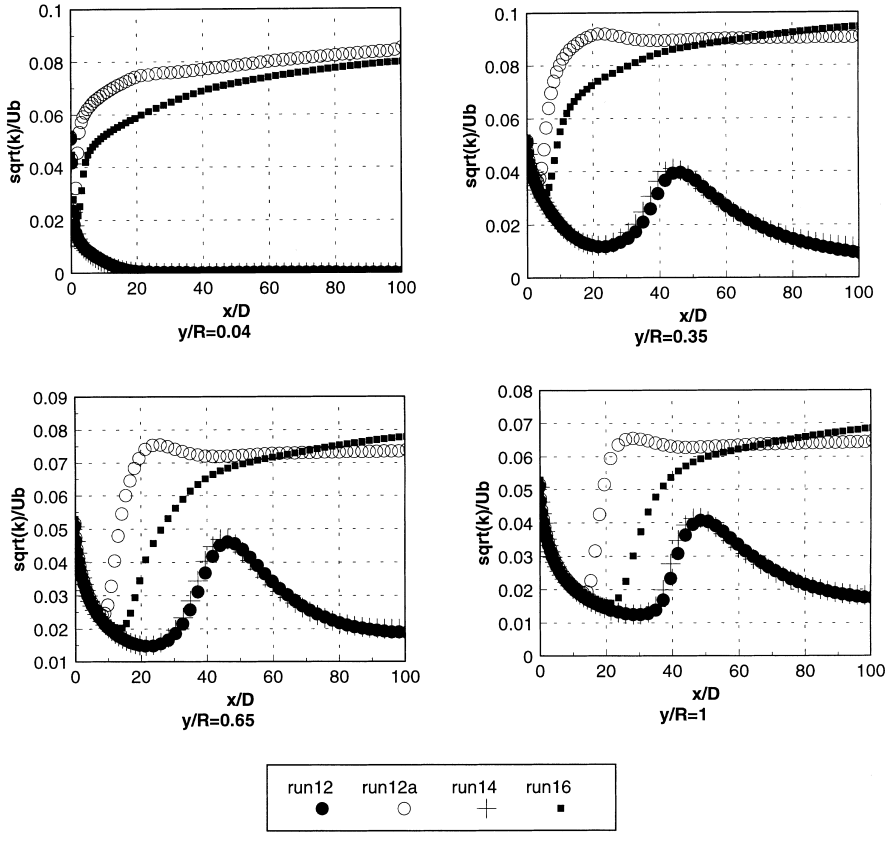

Fig. 11. Variations along the tube of turbulence intensity at chosen radial positions – lower Reynolds number cases ($Re_0 = 4600$).

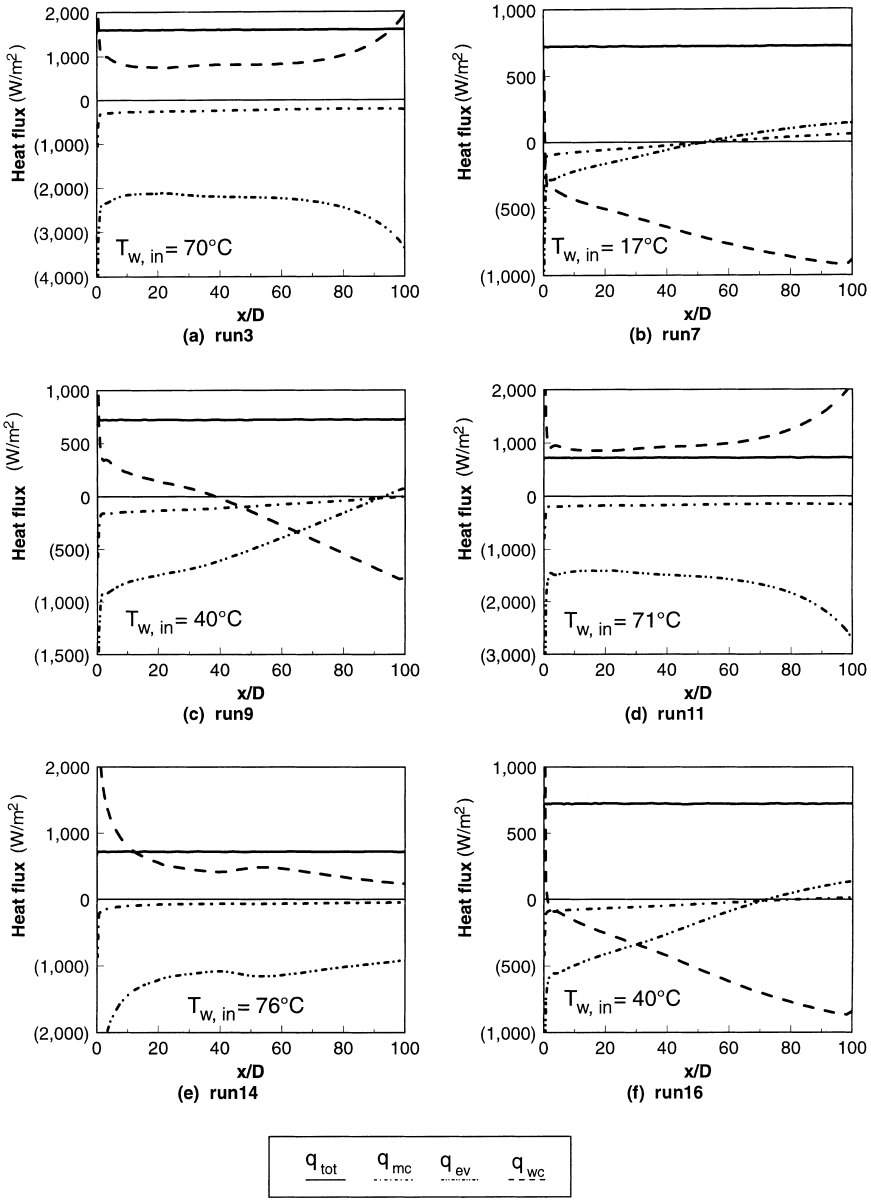

Fig. 12. Energy balance for the water film.

rate of water, the stronger is this effect. Secondly, apart from its dependence on the effectiveness of the transport process, heat transfer due to evaporation is also dependent on the partial pressure of the vapour at the interface. The higher the partial pressure of the vapour, the more vapour is generated at the interface. As shown in Fig. 14, with the increase of temperature, the vapour partial pressure increases strongly and therefore the heat transfer due to evaporation is considerably increased. The results of run 12 and run 12a illustrate this effect; the Nusselt number is reduced by a factor of three in run 12 due to flow laminarisation in comparison with run 12a but the temperature of the wall increases by only about 10°C.

3.3.3. Temperature and vapour concentration fields

Fig. 15 shows the development of temperature profiles in the flow direction for some chosen test cases. Two patterns of development of temperature, corresponding to the two heat transfer modes, can be seen. In the *evaporation mode*, for example runs 3, 11 and 14, the temperature of the water film at inlet is relatively high, the temperature of the wall and that of the air both increase monotonically with distance up the tube. The temperature of the wall is higher than the temperature of the air–vapour mixture at the same cross section and the diffusion of heat is away from the interface. On the other hand, in the *direct film cooling mode*, the temperature of the water at inlet is relatively low. Under such conditions, the temperature of the air/vapour mixture may be higher than the temperature of the wall in the upper section of the tube at the same axial position (see for example, run 7 and run 16). Then, the diffusion of heat is from the mixture towards the interface.

The effect of buoyancy can also be seen from Fig. 15. As an example let us compare the temperature profiles in the upper sections of run 3 (weak buoyancy effect) and run 14 (strong buoyancy effect). It can be clearly seen that run 3 has a temperature distribution typical of turbulent forced convection. The fluid temperature drops deeply in a region near the interface. Outside this region, turbulent mixing is strong and the

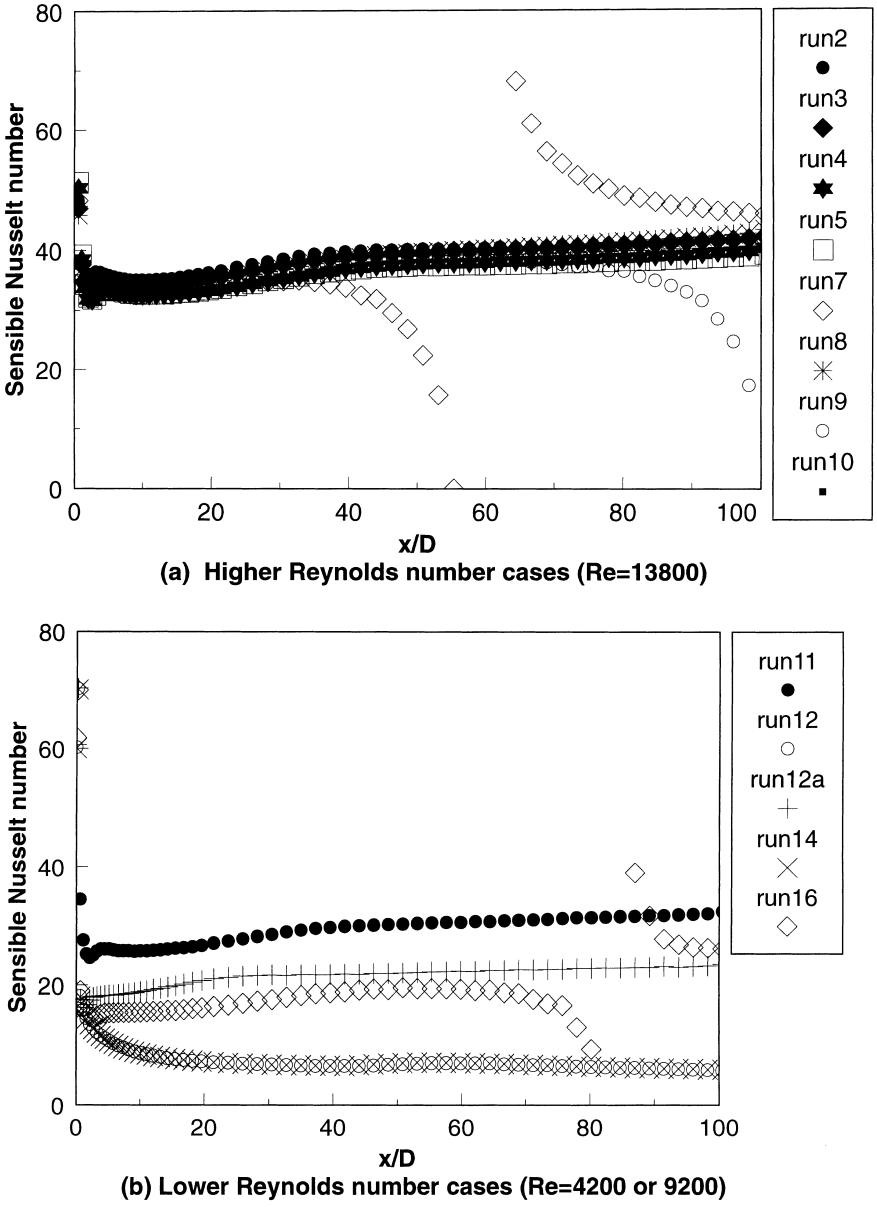

Fig. 13. Variations of sensible Nusselt number along the tube.

temperature gradients are much smaller. In run 14 however, the region where temperature gradient is steep extends much further towards the centre of the tube, indicating that in this region, turbulent diffusion is poor.

Fig. 16 shows radial distributions of vapour concentration along the whole length of the tube for cases corresponding to those shown in Fig. 15. It can be clearly seen that the vapour concentration is high when the system is working in the *evaporation mode* (runs 3, 11 and 14). From the gradient of concentration it is apparent that vapour is being transmitted away from the water film surface at all locations along the tube. In other cases (runs 7, 9 and 16), the vapour concentration at the interface is much lower. From the gradient of concentration, it can be seen that vapour is being transported away from the water film surface in the lower part of the tube and towards it in the upper section. Thus the water is being evaporated from the film in the lower section and vapour is condensing on the film in the upper section.

4. Conclusions

Modelling procedures have been developed which enabled satisfactory simulations to be made of the water film cooling experiments conducted by the present authors. These involved flow in a vertical pipe with heat and mass transfer influenced in some cases by buoyancy. Some very useful understanding of the fluid dynamics and heat transfer physics involved in the problem studied was obtained. The main conclusions from the study are summarised below.

The Launder–Sharma turbulence model is generally able to respond well to the influences present on turbulence under the forced and mixed convection conditions prevailing in the complex combined heat and mass situation considered in this study. However, there is an evidence that under certain situations that turbulence model over-responds to the buoyancy influences and causes laminarisation of the flow to be predicted in the simulations when it does not appear to happen in

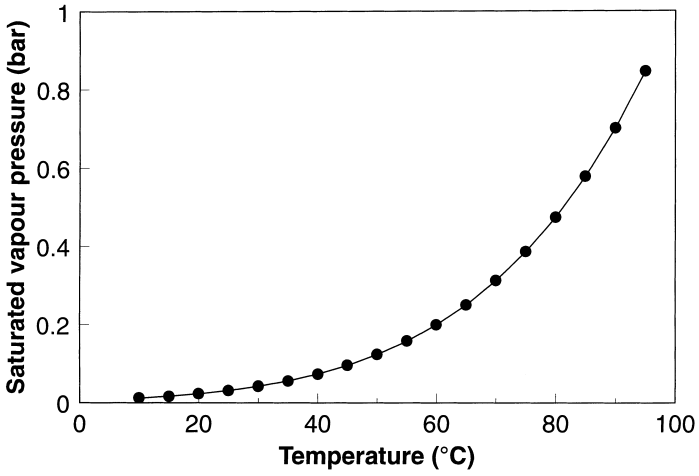

Fig. 14. Variation of the saturation pressure of vapour with temperature.

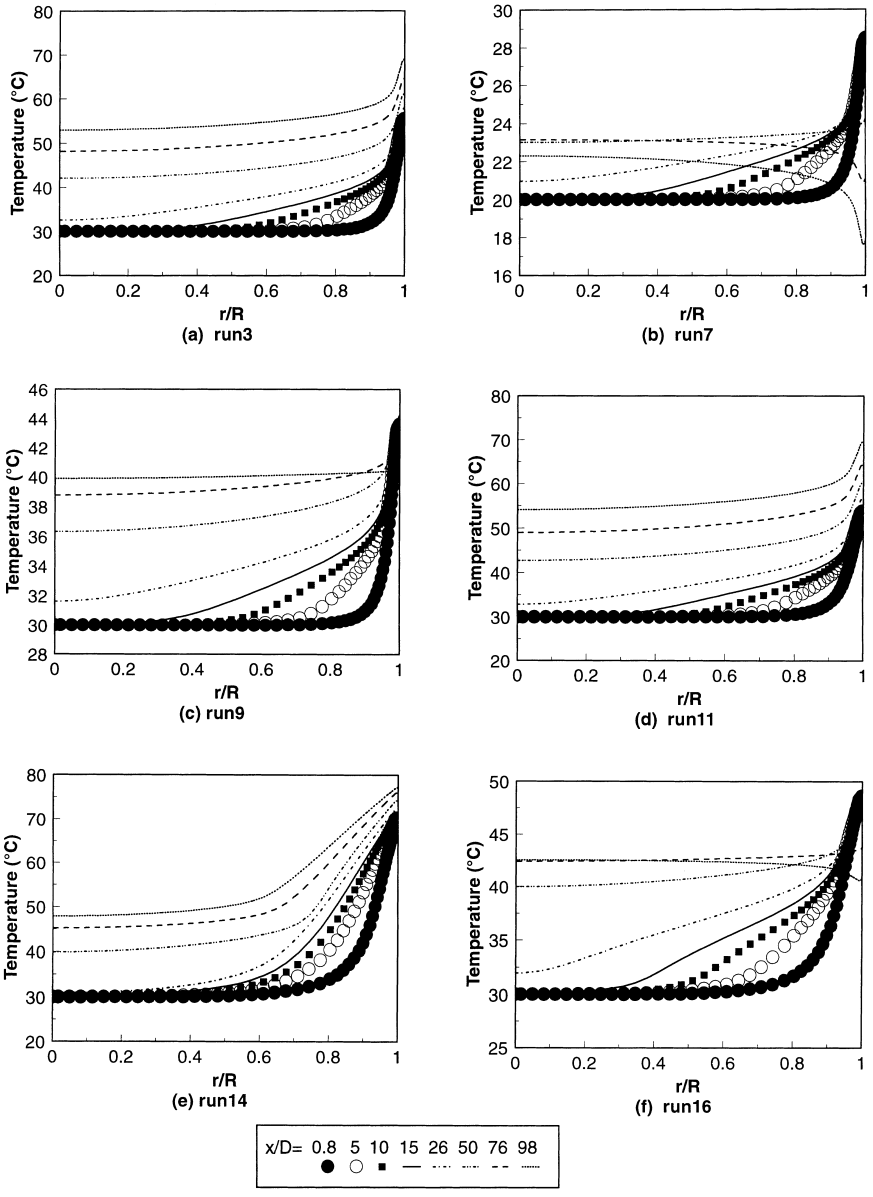

Fig. 15. Development of temperature profiles along the tube.

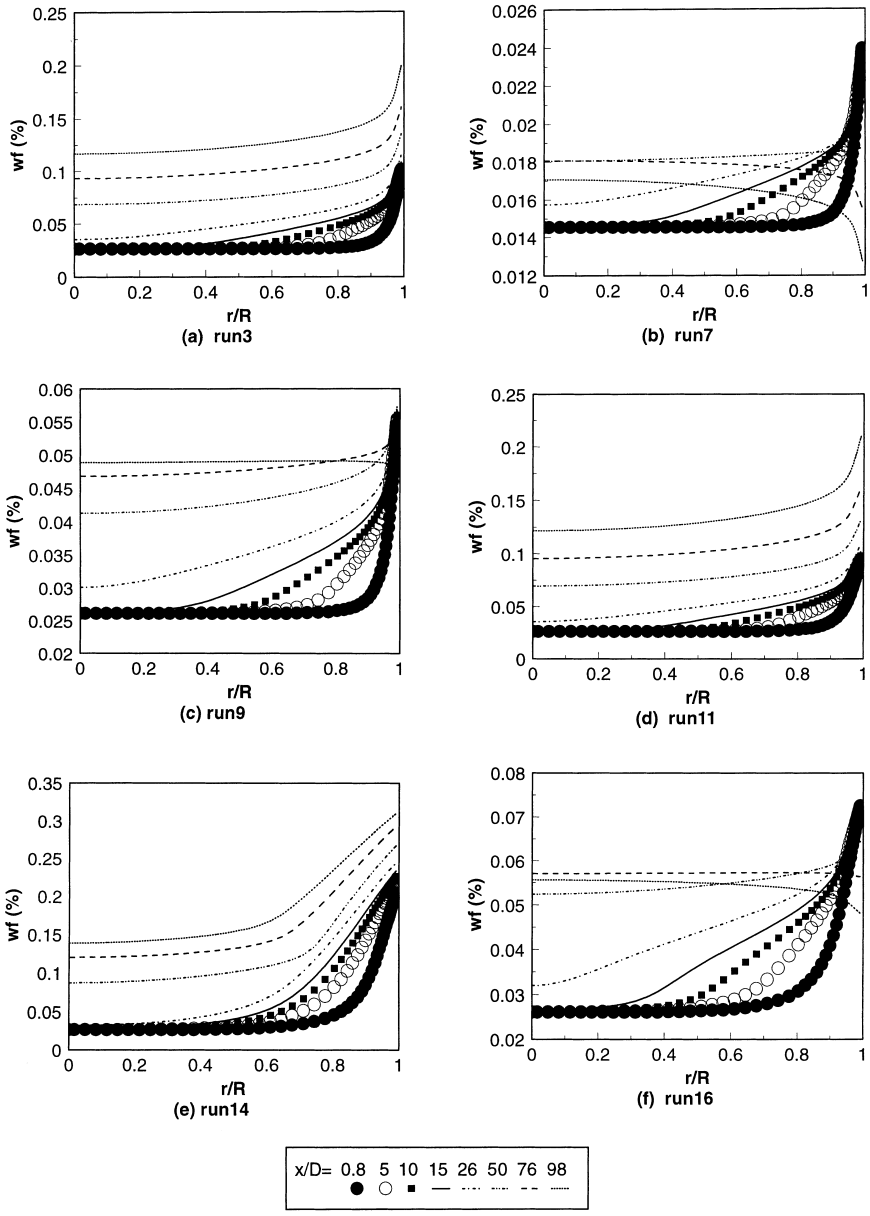

Fig. 16. Development of radial distribution of vapour concentration along the tube.

practice – the model predicts a transition from turbulence to laminar too early.

The flow involved in a heated tube with water film cooling is mainly characterised by two features. Firstly, within the first 20 diameters of tube length, the re-organisation of the mean flow and turbulence field dominates. The initial imposed inlet profiles change towards 'developed turbulent profiles'. Within this region, turbulence brought in with the incoming flow generally decays away. New turbulence is generated in the wall region and this propagates into the core further downstream. The sensible Nusselt number in this region is generally lower than it is in the upper section of the tube. Secondly, in a few cases, both the mean flow and the turbulence fields are affected by the buoyancy forces present which arise due to the non-uniformity of fluid temperature and also vapour concentration. The magnitude of the effect can be characterised by a modified buoyancy parameter, $Bo = 8x10^4\,Gr'/Re_e^{2.625}\,Pr^{0.8}$, in which $Gr' = ((\rho_b - \rho_w)/\rho_b)(gd^3/v^2)$. When this parameter is large, the buoyancy effect is strong and turbulence can be attenuated. Under extreme conditions, the flow undergoes laminarisation, i.e., the turbulence is greatly reduced. Heat transfer is then considerably impaired. However, the increase of wall temperature caused by this effect is generally much less than it would be in a corresponding single phase flow, as explained in the text. It has also be found that in most of the test cases (with the wall temperature being reasonably high), the variations of Reynolds number and the buoyancy parameter along the tube are in the opposite sense to that occurring in single phase flow cases. Reynolds number increases along the tube due to the evaporation of water from the film and the buoyancy parameter decreases.

Two very different modes of heat transfer have been identified, the *evaporation mode* and the *direct film cooling mode*. When the cooling water is supplied at relatively high temperature, the system operates in the *evaporation mode*. Energy supplied by the wall is mainly absorbed by evaporation of liquid

from the water film. The water temperature (which determines the saturated vapour pressure at the water–air interface) and the air/vapour flow rate (which determines the effectiveness of turbulent diffusion of heat and vapour away from the film surface) are both important factors controlling the effectiveness of heat transfer under such conditions. An increase in the rate at which water is supplied to the system generally leads to an increase of wall temperature.

In contrast, when the temperature at which the water is supplied is relatively low, the system operates in the *direct film cooling mode*. The convection of heat by the flowing water film becomes the main mechanism for heat removal from the wall. Only a small part of the heat input to the water passes to the air/vapour mixture. The greater the mass flow rate of water, the lower is the wall temperature. Under such conditions, a change of flow conditions does not significantly affect the heat transfer process.

References

Chang, C.J., Lin, T.F., Yan, W.M., 1986. Natural convection flows in a vertical, open tube resulting from combined buoyancy effects of thermal and mass diffusion. Int. J. Heat Mass Transfer 29 (10), 1543–1552.

Chen, T.S., Yuh, C.F., 1980. Combined heat and mass transfer in natural convection along a vertical cylinder. Int. J. Heat Mass transfer 23, 451–461.

Chiang, H., Kleinstreuer, C., 1991. Analysis of passive cooling in a vertical finite channel using a falling liquid film and buoyancy-induced gas–vapour flow. Int. J. Heat Mass Transfer 34 (9), 2339–2349.

Fedorov, A.G., Viskanta, R., Mohamad, A.A., 1997. Turbulent heat and mass transfer in an asymmetrically heated, vertical parallel-plate channel. Int. J. Heat and Fluid Flow 18, 307–315.

Gebhart, B., Pera, L., 1971. The nature of vertical natural convection flows resulting from the combined buoyancy effects of thermal and mass diffusion. Int. J. Heat Mass Transfer 14, 2025–2050.

Jackson, J.D., An, P., Li, L., 1998. Turbulent heat and mass transfer in a vertical tube with an ascending flow of air and a descending water film. To be presented at Turbulent Heat Transfer-2, Manchester.

Jackson, J.D., Hall, W.B., 1979. Influences of buoyancy on heat transfer to fluids flowing in vertical tubes under turbulent conditions. In: Kakac, S., Spalding, D.B. (Eds.), Turbulent Forced Convection in Channels and Bundles Theory and Applications to Heat Exchangers and Nuclear Reactors, vol. 2, Advanced Study Institute Book, pp. 613–640.

Jackson, J.D., Li, J., 1995. Numerical simulations of variable property, buoyancy-influenced turbulent convection in a heated tube. Proc. CFD95, Banff, Canada.

Jackson, J.D., Mikielewicz, D.P., Poskas, P., 1993. Comparative study of turbulence models against some recent experimental data on buoyancy-influenced heat transfer for ascending flow of air in a tube. Eurotherm Meeting No. 32, On Heat Transfer in Single Phase Flow, Oxford University.

Launder, B.E., Sharma, B.I., 1974. Application of the energy-dissipation of turbulence to calculation of low Reynolds number flow near a spinning disc. Lett. Heat Mass Transfer 1, 131–138.

Patankar, S.V., 1981. A calculation procedure for two-dimensional elliptic situations. Numerical Heat Transfer 4, 409–425.

Ueda, T., Tanaka, H., 1975. Measurement of velocity, temperature and velocity fluctuation distributions in liquid films. Int. J. Multiphase flow 2, 261–272.

Yan, W.M., Lin, T.F., 1990. Combined heat and mass transfer in natural convection between vertical parallel plates with film evaporation. Int. J. Heat and Mass Transfer 33 (3), 529–541.

Yan, W.M., Soong, C.-Y., 1995. Convective heat and mass transfer along an inclined heated plate with film evaporation. Int. J. Heat and Mass Transfer 38 (7), 1261–1269.